Multichannel quantum-defect theory of double-minimum $^1\Sigma_g^+$ states in H_2. I. Potential-energy curves

S. C. Ross
Department of Physics, University of New Brunswick, P.O. Box 4400, Fredericton, New Brunswick, Canada E3B 5A3

Ch. Jungen
Laboratoire Aimé Cotton du CNRS, Université de Paris–Sud, 91405 Orsay, France
(Received 11 November 1993)

Multichannel quantum-defect theory is applied to the highly accurate $^1\Sigma_g^+$ *ab initio* excited-state potential-energy curves calculated by Wolniewicz and Dressler [J. Chem. Phys. **82**, 3262 (1985); and (private communication)]. We show that the three double-minimum states, *EF*, *GK*, and $H\bar{H}$, can be represented to within 8 cm^{-1} by a smooth *R*-dependent 3×3 nondiagonal quantum-defect matrix. This quantum-defect matrix corresponds to a collision of the Rydberg electron with the H_2^+ target, which may be in either the $1\sigma_g$ or $1\sigma_u$ state. Also discussed is the use of this quantum-defect matrix to calculate diabatic states, more highly excited Born-Oppenheimer states, and the electronic ionization width of the superexcited $(1\sigma_u)^2$ doubly excited state.

PACS number(s): 33.10.Cs, 33.10.Lb, 34.10.+x, 34.80.Kw

I. INTRODUCTION

The excited $^1\Sigma_g^+$ states of H_2 are prototype examples of molecular double-minimum states exhibiting effects of strong nonadiabatic coupling. Ever since Davidson [1] recognized the double-minimum nature of the lowest excited electronic energy curve of H_2, $EF\ ^1\Sigma_g^+$, these states have attracted the attention and inspired the imagination of molecular theorists. For example, current models used to explain certain types of persistent hole burning in glasses invoke double-minimum potentials of the same shape as those found in the manifold of excited $^1\Sigma_g$ electronic states of H_2 shown in Fig. 1 [2]. It is known since

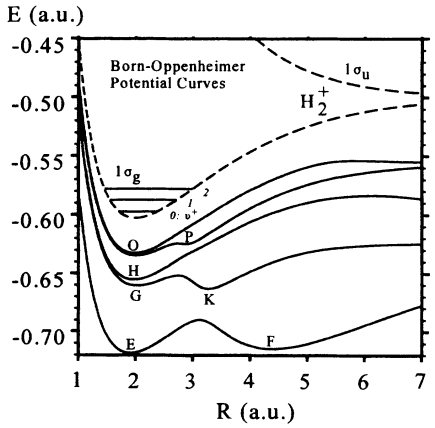

FIG. 1. The *ab initio* Born-Oppenheimer potentials for the first five excited $^1\Sigma_g^+$ states of H_2 (solid curves) [15], along with the spectroscopic labels. The $1\sigma_g$ and $1\sigma_u$ states of H_2^+ (dashed curves), with horizontal lines indicating the lowest vibrational levels of $1\sigma_g$ H_2^+.

Davidson's work that the humps and shoulders which arise in these excited states are the result of avoided crossings that occur between the singly excited Rydberg *s* and *d* series and the doubly excited $(1\sigma_u)^2$ state. In the continuum it is this doubly excited configuration that is largely responsible for the dissociative recombination (DR) of H_2^+ ions with electrons (see, for example, Ref. [3]). DR is an inelastic-scattering process dominated by resonances and proceeding through the temporary formation of H_2 Rydberg states [3]. The strong interaction between the doubly excited state and the singly excited series maintains its importance below threshold, where it is the source of the very large (up to several hundreds of cm^{-1}) non-Born-Oppenheimer effects on the rovibronic levels of H_2. Multichannel quantum-defect theory (MQDT) forms an ideal theoretical description of resonant continuum processes, such as DR [3], as well as of the strongly interacting bound states. This paper is the first in a series which will use MQDT to describe this interaction between a doubly excited state and series of Rydberg states in a unified manner, thus accounting for the possibility of electronic excitation of the ion core when the Rydberg electron collides with it. An early version of this work [4] served as a "proof-of-principle," giving confidence that a careful implementation would be successful in describing the host of short-range interactions that occur when a Rydberg electron collides with an ion core.

It has recently become possible to calculate *ab initio* the electronic energies of the excited states of H_2 with almost spectroscopic accuracy, and also to calculate the strongly perturbed rovibronic structure associated with them. Wolniewicz, Dressler, and co-workers have performed high quality *ab initio* calculations of the $2\ ^1\Sigma_g^+(EF)$, $3\ ^1\Sigma_g^+(GK)$, and $4\ ^1\Sigma_g^+(H\bar{H})$ states [5]. Their calculation of the rovibronic level structures [6] starts out from the Born-Oppenheimer approximation and intro-

duces adiabatic and nonadiabatic coupling terms on a state-by-state basis. The quality of their results, in particular the unprecedented agreement with experiment of their calculated rovibronic levels of H_2, is such that these calculations form a benchmark against which any other theoretical calculations must be compared. This we will do in the following paper [25], where we calculate the vibronic energies of $^1\Sigma_g^+$ H_2, and compare our results with those of Wolniewicz and Dressler.

Our previous calculation accounted explicitly for the strong electronic interaction between singly and doubly excited channels [4]. It was based on a determination of a partial quantum-defect matrix for $^1\Sigma_g^+$ H_2 using the *ab initio* clamped-nuclei (i.e., Born-Oppenheimer) potential curves of Ref. [5] as input data. The quantum-defect matrix obtained there included terms describing the stronger of the electronic channel interactions and correctly accounted for the bulk of the molecular dynamics affecting the vibronic-energy levels of the molecule. A special aspect of the approach we presented in Ref. [4] was that molecular electronic channel interactions were included in a nonperturbative fashion, whereas all previous MQDT treatments (such as that presented in Ref. [3] for DR) were based on a perturbation expansion. The nonperturbative or "direct" feature of our treatment is central to our project and its continuation.

The initial goal of the present work, and the object of this paper, is the *accurate* representation of the improved clamped-nuclei (i.e., Born-Oppenheimer) potential curves [7] shown in Fig. 1 by a set of smooth quantum-defect functions with a well-behaved energy dependence. Jungen and Atabek [8] showed that in the absence of electronic excitation of the core a set of R-dependent quantum-defect *functions* contains all the information necessary to describe the breakdown of the Born-Oppenheimer approximation that occurs during the collision of the Rydberg electron with the vibrating-rotating H_2^+ ion core. In later papers in this series we shall show that when electronic core excitation occurs it is the *matrix* of quantum-defect functions that allows an essentially complete description of the electron-ion collision, including the coupling of nuclear and electronic motion. The present paper is concerned with the determination and evaluation of this matrix of quantum-defect functions.

II. THEORY

We consider the 2, 3, and 4 $^1\Sigma_g^+$ electronic states of H_2, which are also known as the EF, GK, and $H\bar{H}$ states. The "clamped-nuclei" or Born-Oppenheimer potential-energy curves of these states are shown in Fig. 1. This figure presents a complicated pattern of avoided crossings between the s and d Rydberg series on one hand, and the $(1\sigma_u)^2$ doubly excited state on the other. The strength of the interaction between these states can be seen to be considerable. Our goal is to use multichannel quantum-defect theory (MQDT) to obtain a theoretical description of this system. Although detailed descriptions of MQDT are available in several review papers [9–11], in the current series of papers we shall present a concise summary of the theory as we apply it.

We start with the simple intuitive picture of series of crossing diabatic states such as those shown in Fig. 2. Each series of diabatic states is considered as being describable as a single configuration and thus by a single quantum-defect function. In the present case, we label the diabatic series as

$$s\colon\ (1\sigma_g)ns\sigma_g,\quad d\colon\ (1\sigma_g)nd\sigma_g,\quad p\colon\ (1\sigma_u)np\sigma_u\ .$$

Thus, in this notation, we label the doubly excited configuration $(1\sigma_u)^2$ as $(1\sigma_u)(2p\sigma_u)$. Configuration interaction between these diabatic series leads to the avoided crossings and thus to the complicated pattern of energy curves shown in Fig. 1. For each pair of series there is an additional quantum-defect function corresponding to their interaction. In our present problem we thus have to determine three diagonal quantum-defect functions, $\eta_{ss}(R)$, $\eta_{dd}(R)$, and $\eta_{pp}(R)$, describing the s, d, and p diabatic series, and three off-diagonal quantum-defect functions, $\eta_{sd}(R)$, $\eta_{sp}(R)$, and $\eta_{dp}(R)$, describing the interactions between these series.

The quantum-defect theory (QDT) description of an electronically excited atom or molecule describes the atom or molecule as an electron (the Rydberg electron) in collision with a positively charged ion core. This is reflected in the QDT wave functions, wherein the radial motion of the colliding Rydberg electron is distinguished from the other degrees of freedom of the molecule. Outside some finite radius r_0, QDT assumes that the Rydberg electron sees only the spherically symmetric Coulomb force of the positively charged ion core and, thus, the radial part of the wave function corresponding to the Rydberg electron can be written as a linear combination of a base pair of energy-dependent Coulomb functions. In our work, we choose the Coulomb base pair $f_l(r)$ (regular at the origin) and $h_l(r)$ (irregular at the origin) [9], where l

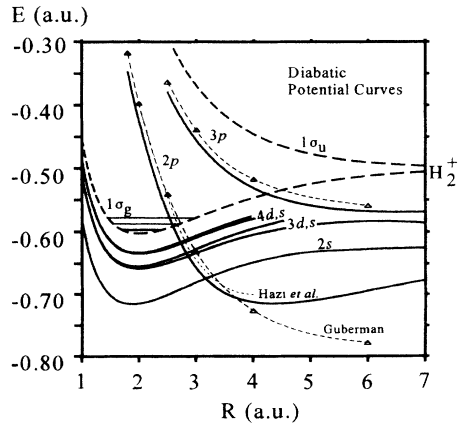

FIG. 2. Diabatic potential curves from the present MQDT analysis (solid curves) along with results from Guberman [22] (triangles connected by dashed line) and Hazi, Derkits, and Bardsley [16] (thin dashed curve). Note that 3s and 4s lie *above* 3d and 4d, respectively. H_2^+ as in Fig. 1.

is the angular-momentum quantum number of the Rydberg electron and r is the distance from the center of the H_2 molecule to the Rydberg electron. In a one channel problem the molecular QDT wave function for $r \geq r_0$ and clamped nuclei involves a linear combination of $f_l(r)$ and $h_l(r)$ and is written,

$$\Psi(\theta,R,r)=\psi(\theta,R)\{f_l(r)+\tan[\pi\eta(R)]h_l(r)\} . \quad (1)$$

Here, θ represents all degrees of freedom of the molecule other than the internuclear distance, R, and the radial coordinate of the Rydberg electron, r. The quantum-defect function $\eta(R)$, is seen in Eq. (1) to represent the linear combination of the $f_l(r)$ and $h_l(r)$ functions appearing in the wave function. If there are no electrons in the ion core this function must be valid down to $r=0$ when $R=0$. Combined with the irregularity of $h_l(r)$ at the origin this has the consequence that only the regular function $f_l(r)$ can appear in the wave function. Thus, the absence of core electrons forces $\eta(R=0)$ to be zero. If there are electrons in the ion core then the collision of the Rydberg electron with them may result in some amount of the irregular $h_l(r)$ functions appearing in the wave function with the consequence that even at $R=0$ the quantum defect may be different from zero. The quantum-defect function is thus seen to be a measure of the interaction of the Rydberg electron with the core. Because this interaction depends on the exact configuration of the core, the quantum defect is a function of the internuclear distance, R.

A special feature of QDT is that the bound-state boundary condition is *not* imposed on the radial function of the Rydberg electron at the outset. Instead advantage is taken of the fact that the Coulomb functions $f_l(r)$ and $h_l(r)$ are defined at any energy, ϵ, of the Rydberg electron. This naturally gives rise to the concept of a channel wherein the discrete set of principal quantum numbers of the diabatic series is replaced by the continuous variable ϵ. Thus, the three diabatic series of the current problem are replaced by the three channels,

$$s\colon\ (1\sigma_g)\epsilon s\sigma_g,\quad d\colon\ (1\sigma_g)\epsilon d\sigma_g,\quad p\colon\ (1\sigma_u)\epsilon p\sigma_u .$$

Because the energy of the Rydberg electron is left unspecified, each of these channels includes an entire diabatic Rydberg series along with the associated continuum lying above. The relation between the total energy E of the molecule, the energy $E_i^+(R)$ of the ion core, and the energy ϵ_i of the Rydberg electron in channel i is

$$\epsilon_i(R)=E-E_i(R) , \quad (2)$$

where i indexes the ion-core state. For negative ϵ_i the "effective quantum number" ν is given by

$$\nu_i(R)=\left[-\frac{1}{2\epsilon_i(R)}\right]^{1/2} , \quad (3)$$

where ν, like ϵ, depends on the internuclear spacing R and the state of the ion core.

If the bound-state boundary condition $\Psi(\theta,R\rightarrow\infty)=0$, is imposed on the wave function of Eq. (1), then the asymptotic forms of the $f_l(r)$ and $h_l(r)$ functions require [9]

$$0=\left|\tan[\pi\eta(R)]+\frac{\tan[\pi\nu(R)]}{A_l(\nu(R))}\right| , \quad (4)$$

where

$$A_l(\nu)=\prod_{j=0}^{l}\left[1-\frac{j^2}{\nu^2}\right] . \quad (5)$$

$A_l(\nu)$ appears in Eq. (4) because of our use of the $h_l(r)$ function and related η quantum defect, instead of the more commonly used $g_l(r)$ Coulomb function and associated μ quantum defect.

If the energy $E_i^+(R)$ of the ion state and the quantum defect $\eta(R)$ are known for some value of R, then the total energy E can be scanned to search for eigenvalues. This is done by using Eqs. (3) and (5) to determine ν and $A_l(\nu)$, respectively, and hence to evaluate the right-hand side of Eq. (4). Whenever the result is zero the trial total energy E is indeed an eigenenergy of the molecule for R, corresponding to a clamped-nuclei energy—in other words a Born-Oppenheimer electronic energy for the internuclear spacing R. This procedure can be repeated on a grid of R values and the resulting Born-Oppenheimer potential-energy curves can then be pieced together. Because of the periodic nature of the tangent function there is an infinite number of such curves. These curves are the electronic energy curves of the Rydberg states of the system under consideration.

As shown in Figs. 1 and 2, and as discussed above, the ${}^1\Sigma_g^+$ system of H_2 involves three channels closely coupled by electronic interaction. It is, therefore, necessary to apply a multichannel QDT (MQDT) treatment. The generalization to a multichannel theory is done by starting with a basis set $\{\Psi_i\}$ that, for each channel i, explicitly allows for the admixture of h functions due to the interaction with the ion core. This includes the admixture of h functions from the other channels,

$$\begin{aligned}\Psi_i&=f_i(r)|i\rangle+\sum_j\{\tan[\pi\eta_{ij}(R)]\}h_j(r)|j\rangle\\&=f_i(r)|i\rangle+\sum_j K_{ij}(R)h_j(r)|j\rangle .\end{aligned} \quad (6)$$

The kets in this expression represent all degrees of freedom of the molecule other than the radial motion of the Rydberg electron. The K matrix,

$$K_{ij}(R)=\tan[\pi\eta_{ij}(R)] , \quad (7)$$

is called the reaction matrix and it is this matrix that introduces into MQDT the possibility of electronic interaction between the various channels. The K matrix of MQDT must be distinguished from the physical reaction matrix $K(E)$. The MQDT reaction matrix, K, may explicitly include closed channels, whereas $K(E)$ does not. It is this that allows the MQDT K matrix to be a smooth function of energy. The singularities that appear in $K(E)$ and also in the scattering matrix actually arise from the elimination of the closed channels. In the energy range

that we consider in the present paper all of the channels that we include are closed.

The total wave function for the molecule is expressed as a linear combination of the Ψ_i basis functions of Eq. (6),

$$\Psi=\sum_i Z_i\Psi_i \ . \tag{8}$$

The asymptotic forms of the f and h functions imply that the bound-state boundary condition $\Psi(r\rightarrow\infty)=0$ is only satisfied if the following well-known determinantal equation is satisfied [9],

$$\left|K+\frac{\tan(\pi\nu)}{A(\nu)}\right|=0 \ , \tag{9}$$

where K is given by Eq. (7) and $\tan\pi\nu$ and $A(\nu)$ are the diagonal matrices

$$\begin{aligned}&[\tan(\pi\nu)]_{i,j}=\delta_{ij}\tan(\pi\nu)_i \ ,\\ &[A(\nu)]_{i,j}=\delta_{ij}A_{l_i}(\nu_i) \ .\end{aligned} \tag{10}$$

Thus, the multichannel equation, Eq. (9), is identical in form to that of the single channel given in Eq. (4).

If the quantum-defect matrix $\eta_{ij}(R)$ is known then the Born-Oppenheimer potential-energy curves can be obtained by the same procedure as was outlined above for the single-channel case.

In this work we proceed in the opposite direction, determining the quantum defects for $^1\Sigma_g^+$ H_2 from the high quality H_2 *ab initio* Born-Oppenheimer potential curves of Wolniewicz and Dressler [5,7], combined with those of $1\sigma_g$ and $1\sigma_u H_2^+$ from the work of Wind [12] and Bates, Ledsham, and Stewart [13] respectively. Because there are three channels involved in this system the symmetric K and η matrices involve six independent elements.

One final point that should be mentioned is the reason for the choice of the Coulomb basis pair f and h, rather than the more common pair f and g. Seaton [9] devised the h function so as to avoid the appearance of nonphysical states with $n<l+1$, such as $1p$, $1d$, $2d$, etc., that show up when the f and g pair is used. This is particularly important in the $^1\Sigma_g^+$ system of H_2 because the nonphysical $2d$ state would cross through the region of the double minimum of the *EF* state and hence would interact with the physical states lying in its path, thus rendering impossible the MQDT approach.

III. DETERMINATION OF THE QUANTUM-DEFECT MATRIX

The relevant high quality *ab initio* data available for the determination of the elements of the quantum-defect matrix only includes the three states: 2, 3, and $4\,^1\Sigma_g^+$ [5,7]. The problem at each R value is, therefore, underdetermined at the outset since we have six quantum defects to determine from only three items of data. *Ab initio* calculations for higher states would therefore be very useful for the determination of the quantum-defect curves and their energy dependence. Our approach has been to use the data that are available to determine the quantum-defect matrix for *all* R values simultaneously in a least-squares fitting procedure. We are able to do this because we impose the constraint that each element must be a smooth function of the molecular bond length R. Additional constraints were imposed on the individual quantum-defect functions for the limits $R\rightarrow 0$ and $R\rightarrow\infty$. We now discuss in turn the diagonal elements $\eta_{ii}(R)$, the off-diagonal elements $\eta_{ij}(R)$, and the energy dependence of these elements.

A. $\eta_{ii}(R)$—diagonal quantum defects

Each diabatic Rydberg series i is described by the corresponding diagonal element of the quantum-defect matrix, $\eta_{ii}(R)$. We force the $\eta_{ii}(R)$ to be smooth functions by using their values at several widely spaced R values as the parameters defining the function. Cubic spline interpolation is then used to determine the $\eta_{ii}(R)$ between the fitted points. In this way we represent the continuous curve by a small number of parameters suitable for fitting, at the same time ensuring a reasonable degree of smoothness in the resulting quantum defects.

The following constraints were imposed on the $\eta_{ii}(R)$. First, one of the parameters for each diagonal defect was its value at $R=\infty$, corresponding to the physical limit of two separated hydrogen atoms. For the purpose of spline interpolation the value of η_{ii} at $R=15$ a.u. was set to this known value and was not adjusted during the least-squares fitting. Second, since $R\rightarrow 0$ corresponds to the physical limit of a helium atom, the parameters $\eta_{ss}(R=0)$ and $\eta_{dd}(R=0)$ were set to values determined from a QDT fitting to the observed s and d channel energies of the helium atom. In helium, it is the state $(2p)^2$ that corresponds to the $(1\sigma_u)(\epsilon p\sigma_u)$ channel. This state, however, is embedded in the continuum of the s and d channels and lies so high in energy that it is not relevant to the energy range being considered here. Because of this $\eta_{pp}(R=0)$ was not used as a parameter.

B. $\eta_{i\neq j}(R)$—off-diagonal quantum defects

The off-diagonal elements of the η matrix describe the interchannel coupling and are related to the avoided crossings of Fig. 1. In our previous work [4], we only determined the two strongest coupling elements, η_{sp} and η_{dp}. In that work, these elements were forced to zero outside the region of the avoided crossings of Fig. 1, and we determined their values at many points from $R=2.5$ to 3.5 a.u. In the current work, initial fittings of η_{sp} and η_{dp} in the interaction region showed these functions to be almost constant. We have taken advantage of this by modeling these coupling elements as exactly constant over this interval. Since neither the Born-Oppenheimer potential-energy curves nor any experimental data yet available supply information about the values of these interactions for values of $R\leq 2$ a.u., we have simply extended the constant values of η_{sp} and η_{dp} down to $R=0$. This may have some consequences for the use of the fitted quantum defects to predict higher states. This simplification of the modeling of η_{sp} and η_{dp} has allowed

us to include the weaker η_{sd} mixing element in the least-squares fitting as well.

It is known (see Mulliken [14]) that for large R values further complications arise in that avoided crossings additional to those shown in Figs. 1 and 2 occur on the way to dissociation. One of these is considered in the Discussion. For our current purposes, however, we have restricted our treatment to the region of strong interactions near R_e and have, therefore, not maintained the channel interactions out to $R \rightarrow \infty$. Instead we assume that for $R \geq 7$ a.u. the molecule moves adiabatically, with no electronic mixing between the channels. We arbitrarily chose to turn off the constant η_{sp} and η_{dp} interactions beyond this distance by smoothly matching them to zero between $R=5$ and 7 a.u., and by then continuing them as zero from $R=7$ to ∞ a.u. This was done by using a cubic interpolation between their fitted constant nonzero values for $R \leq 5$ a.u. and the constant value of zero for $R \geq 7$ a.u. Because of this simple modeling η_{sp} and η_{dp} were, therefore, each described by a single parameter, their constant values in the region $R=0-5$ a.u., which were determined in the simultaneous least-squares fitting.

With these constraints on η_{sp} and η_{dp} it was then possible to fit the smaller sd mixing term η_{sd}. Again there is a physical constraint to be imposed. In the limit $R \rightarrow 0$, the system becomes that of the spherically symmetric helium atom. Because spherical symmetry is not preserved in a one electron interaction, the fact that the s and d channels are built on the same core means that we must set $\eta_{sd}(R=0)=0$. The p channel, however, is built on a different core, so that the interactions between it and the s and d channels are two electron interactions, which can preserve spherical symmetry. Thus, neither η_{sp} nor η_{dp} were forced to zero for $R=0$. Additionally, we force η_{sd} to zero for $R \geq 6$, almost the same arbitrary region as we used for η_{sp} and η_{dp}. For $R<6$ a.u., η_{sd} was modeled by a cubic spline function in the same way as were the diagonal quantum defects. We chose four points in the interval $r=1.4-4.0$ a.u. for which η_{sd} was determined in the least-squares-fitting procedure.

It must be stressed that forcing the off-diagonal quantum defects to zero at large R has consequences for the physical meaning of the fitted quantum-defect matrix. In particular, it must be remembered that a partial wave expansion based on the quantum defects determined here would not be physical for R greater than about 5 a.u.

C. Energy dependence

The *ab initio* data available only supported the determination of the energy dependence of the η_{ss} element of the η matrix. This determination was possible because *ab initio* Born-Oppenheimer curves were available for both the E and H states which, for values of R smaller than those in the region of the avoided crossings, may be approximately identified as the $2s$ and $3s$ states, respectively. With only two states available the obvious choice was to model the energy dependence by choosing the η_{ss} defect to be a linear function of the energy ϵ of the Rydberg electron,

$$\eta_{ss}(\epsilon)=\eta_{ss}^{(0)}+\eta_{ss}^{(1)}\epsilon \ , \tag{11}$$

where this energy dependence and, thus, the two coefficients of Eq. (11), $\eta_{ss}^{(0)}$ and $\eta_{ss}^{(1)}$, are, in principle, functions of the internuclear distance, R.

During the preparation of this manuscript new *ab initio* data [15], including yet higher $^1\Sigma_g^+$ states, were communicated to us. The earlier *ab initio* potential-energy curves [5,7] corresponding to the $2s$ and $3s$ diabatic states had already indicated clearly that the energy dependence of η_{ss} is strikingly R independent for small values of R. With the curves of Ref. 15, which were not available at the time this work was performed, this constant energy dependence of η_{ss} is now seen to extend over the region $R=1.1-2.4$ a.u., and to extend to higher energy to include the $4s$ state. This is most clearly illustrated by calculating $\eta_{ss}(R=1.1-2.4$ a.u.) from the E ($\approx 2s$) *ab initio* data, and then using this quantum defect to predict the higher s potentials, setting all interactions to zero in both steps. Over this range, the resulting predictions for the H ($\approx 3s$) potential-energy curve lie in the narrow window of 54.2–58.4 cm^{-1} below the actual potential-energy curve of the H state. This occurs despite the fact that the potential of the H state varies by more than 20 000 cm^{-1}

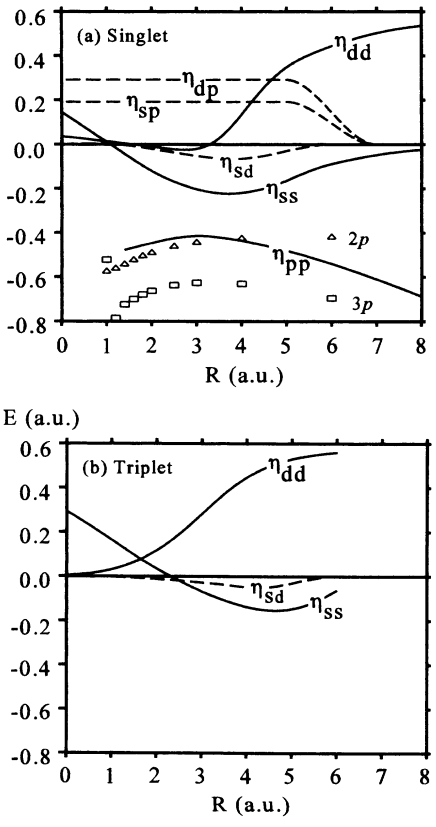

FIG. 3. The elements of the quantum-defect matrix as functions of R (diagonal elements: solid lines, off-diagonal elements: dashed lines). η_{ss} is shown for $\epsilon=0$. (a) $^1\Sigma_g^+$ defects. Note that $\eta_{sd}(R=0)=0$. η_{pp} defects are shown shifted down by 1 to avoid congestion. Values derived from Guberman's [22] calculations of the $2p$ and $3p$ states are shown by triangles and boxes, respectively. (b) $^3\Sigma_g^+$ defects.

over this range. The same procedure applied to the helium atom results in a prediction for the $3s$ state that is 56.0 cm^{-1} below the experimental value, consistent with the value in the H_2 molecule. The E ($\approx 2s$) based prediction for the O ($\approx 4s$) state lies below the *ab initio* curve in the narrow window of 29.5–34.1 cm^{-1}, and in the helium atom the $2s$ prediction of $4s$ is too low by 29.5 cm^{-1}. Thus, the R independence of the energy dependence of η_{ss} extends to higher energy. In Sec. IV we shall see that the linear energy dependence is sufficient to describe η_{ss} from $2s$ to $4s$, an energy range of more than 18 000 cm^{-1}. In addition to providing evidence of the convergence of the new *ab initio* results for the O state, the uniform energy dependence indicates that for small R values it is reasonable to choose the energy-dependence parameter $\eta_{ss}^{(1)}$ as independent of R. We do this over the range $R=0-2$ a.u.

Beyond this distance the $2s$ diabatic curve enters the region of strong configuration interaction. At values of R beyond the region of the strong avoided crossings the only high-quality *ab initio* potential-energy curve available involving the s diabatic series was that of the K state, which we may identify for our purposes as the $2s$ state. This lack of information means that it was not possible to determine the long-range form of η_{ss} energy dependence with the available *ab initio* results. However, in the limit of very large R the system resolves into two hydrogen atoms, in which case the quantum defect does not depend on energy. We therefore forced the linear coefficient of the energy dependence $\eta_{ss}^{(1)}$ to zero for large R by smoothly matching the constant value of $\eta_{ss}^{(1)}$ in the region $R=0-2$ a.u., to the zero value for the region $R=3-\infty$ a.u. This was done using a cubic function in the interval $R=2-3$ a.u. in the same way that η_{sp} and η_{dp} were turned off at large R. This "turning-off" zone of the energy dependence was chosen more or less arbitrarily. In Sec. IV, however, we shall show that the newly available *ab initio* results [15] indicate that this procedure was, in fact, appropriate.

The energy dependence of all the other quantum-defect functions was not determinable with the *ab initio* data available at the time we performed this work. Because of this they were all taken as independent of energy.

D. Least-squares fitting

In our "proof-of-principle" calculation the fitting was neither complete (η_{sd} was fixed to zero) nor simultaneous (a sequence of partial fittings of various subsets of the parameters was performed [4]). In the present work, we performed a simultaneous least-squares fitting of the parameters defining the quantum-defect matrix and its energy dependence. These parameters were fit to improved versions [7] of the *ab initio* potential-energy curves of Wolniewicz and Dressler [5] for the EF, GK, and $H\bar{H}$ states for $R \geq 1.4$ a.u. Figure 3(a) shows the elements of the resulting quantum-defect matrix, with η_{ss} shown for $\epsilon=0$ and η_{pp} shifted down by 1 to avoid congestion. Because we neglect the energy dependence of the other defects the curves shown for them in Fig. 3(a) correspond to their values at electron energies corresponding to the EF, GK, and $H\bar{H}$ states. The quantum-defect matrix will be considered in more detail in the Discussion below.

The quality of the fitting is shown by a comparison of the input *ab initio* and the calculated MQDT energies for R from 1.4 to 7.0 a.u. In this region, the rms error over all three potential curves is 1.7 cm^{-1}, with no point worse than 8.0 cm^{-1}. This represents a significant improvement over our previous work wherein the rms error was 4.8 cm^{-1}, and the worst points were as far as 20.7 cm^{-1} from the *ab initio*. For each state the largest discrepancies (in cm^{-1}) in the present work and in our previous work are, respectively, EF (8.0, 20.7), GK (3.4, 15.7), and $H\bar{H}$ (4.4, 18.6).

Hazi, Derkits, and Bardsley [16] have also performed a quantum-defect parametrization of *two* of these same potential-energy curves (EF and GK) in the narrow region $R=2.5-3.5$ a.u. Our present result, involving the simultaneous fitting of *three* of these curves to better than 8.0 cm^{-1}, compares very favorably with their largest discrepancy of approximately 120 cm^{-1}.

IV. DISCUSSION

The quantum-defect matrix shown in Fig. 3(a) reproduces the *ab initio* Born-Oppenheimer potential curves for the EF, GK, and $H\bar{H}$ states to within 8.0 cm^{-1}. On the scale of the energies involved in these states this agreement represents an extremely good fitting. It must, however, be remembered that parameter values determined in a fitting process are, at least to some extent, "effective" values. In other words the fitted values for the parameters may be different from the "true" physical ones, due to the fact that the fitted parameters must account for any effects or terms neglected in the model. Thus the fact that the η matrix of Fig. 3(a) reproduces the Born-Oppenheimer potential curves so well does not, in itself, indicate that this matrix has the physical significance implied by its appearance in the configuration mixed basis functions of Eq. (6). With no further evidence our η matrix serves merely as a parametrization, albeit extremely concise and precise, of the *ab initio* Born-Oppenheimer potential-energy curves.

One important point, however, concerns the ambiguity of the signs of the off-diagonal elements of the K matrix. Because of the nature of the determinant function, Eq. (9) is insensitive to certain changes of sign of the off-diagonal elements of the K matrix. As a consequence the sign of the single off-diagonal element of the 2×2 K matrix determined below for the triplet state [Fig. 3(b)] is indeterminate, while the signs of any pairs of off-diagonal elements of the 3×3 K matrix used for the singlet state [Fig. 3(a)] can be negated without changing the results. This has no consequence *vis a vis* the calculation of vibronic and rovibronic energies, but will play a role in any calculation of intensities.

In the following paper, we present results of calculations of the vibronic levels of the $^1\Sigma_g^+$ states of H_2 using the η matrix determined here. These calculations involve the complicated dynamics of non-Born-Oppenheimer interactions and rely on the representation of the electronic wave functions in terms of the R-dependent η matrix as given in Eqs. (6) and (8). The results we obtain there are

in excellent agreement with experiment, approaching the quality of the best direct state-by-state calculations performed by Dressler and co-workers [6,17]. This is powerful evidence for the physical content of our quantum-defect matrix.

In the remainder of this section we present arguments demonstrating the physicality of our quantum-defect matrix.

A. Triplet Σ_g^+ states

We expect the "true" quantum defects of the triplet $^3\Sigma_g^+$ system of H_2 to be similar to those of the singlet $^1\Sigma_g^+$ system. To investigate whether our fitted defects satisfy this we determined the η matrix for the triplet $^3\Sigma_g^+$ system using the same procedure as described above for the singlet $^1\Sigma_g^+$ system. The only major difference anticipated between the two systems is due to the fact that the Pauli principle forbids the $(1\sigma_u)(2p\sigma_u)=(1\sigma_u)^2$ state in the triplet system. Thus, the lowest $2p$ triplet state is $(1\sigma_u)3p\sigma_u$, which lies well above the energy range we consider in the current work, that of the *EF*, *GK*, and $H\bar{H}$ singlet states. Therefore, in this energy range the strong electronic interactions with the $(1\sigma_u)(2p\sigma_u)$ state do not play a role in the triplet system and as a consequence the strong avoided crossings and double minima due to *sp* and *dp* mixing do not occur here. This permits us to neglect the *p* channel in the triplet system which in turn allows us to clearly determine the relatively small $\eta_{sd}(R)$ defect. The smallness of the *sd* interaction in the triplet system meant that it was only possible to determine one parameter for this quantity. Because η_{sd} must be zero at $R=0$, we have modeled it as a rising quadratic function for $R=0$–4 a.u. (chosen arbitrarily), smoothly matched by a cubic function to zero for $R\geq 6$ a.u. (also chosen arbitrarily). Figure 3(b) shows the elements of the resulting two-by-two quantum-defect matrix determined by fitting to the *ab initio* Born-Oppenheimer potential curves of Refs. [18] and [19] for the triplet system. Comparison of Figs. 3(a) and 3(b) shows that those defects shared by both the singlet and triplet systems have quite similar forms, indicating that it is not unreasonable to assume that they may indeed have physical content.

[Note that the agreement in form of the singlet and triplet $\eta_{sd}(R)$ functions for $R>2$ a.u. is fortuitous. It was possible to obtain an equally good fitting for the triplet state in which η_{sd} was allowed to rise quadratically to $R=2$ a.u., instead of $R=4$ a.u., and then forced to decrease to zero for $R\geq 4$ a.u., instead of for $R\geq 6$ a.u. This results in a triplet $\eta_{sd}(R)$ quantum-defect function that for values of R greater than 2 a.u. is different in form from that shown in Fig. 3(b). The single parameter used to define η_{sd}, $\eta_{sd}(R=2$ a.u.), however, had identical values in both fittings.]

B. Higher Born-Oppenheimer states

The quantum-defect matrix we have determined allows the prediction of both diabatic (crossing) and Born-Oppenheimer (noncrossing) potential-energy curves for higher states. The diabatic curves of Fig. 2 were obtained following the same procedure as used for obtaining the Born-Oppenheimer curves, but with the off-diagonal quantum defects set to zero. Two facts, however, should be remembered. First, the available *ab initio* data only allowed us to determine the energy dependence of the η_{ss} function. All of the other quantum-defect functions were assumed to be independent of energy. Second, we used simple forms for the η_{sp} and η_{dp} off-diagonal quantum-defect functions, forcing them to be constant from $R=0$ to 5 a.u., and then to drop smoothly to zero for $R\geq 7$ a.u. These two constraints must clearly have consequences on the fitted values of the quantum-defect functions, as any resulting error must be subsumed by alterations in the fitted values of the other defects. Despite this it is still possible to make useful predictions of higher states and of the diabatic states, particularly since the consequence in terms of energy of any error in the quantum defects should become progressively smaller with increasing principal quantum number.

Our fitted quantum-defect functions are based on *ab initio* potential-energy curves for the *EF*, *GK*, $H\bar{H}$ (2, 3, and $4\,^1\Sigma_g^+$) states calculated by Wolniewicz and Dressler [5,7]. Their calculations also included preliminary *ab initio* Born-Oppenheimer potential-energy curves for the *P* and *O* (5 and $6\,^1\Sigma_g^+$) states. For certain values of the internuclear spacing these preliminary *P* and *O* state *ab initio* potentials lay to significantly higher energies than predicted by our quantum-defect matrix which was determined from the lower states. It was in part our MQDT predictions that indicated that the *ab initio* calculations for the *P* and *O* states had not yet converged, and lead to improved *ab initio* calculations. In the course of the preparation of this manuscript Wolniewicz and Dressler communicated to us the results of their new *ab initio* calculations for the *P* and *O* states [15]. These potentials, which we have already mentioned in Sec. III C, are believed to be well converged. In the future, they may serve as extremely useful input for further improvement of our electronic K matrix. In particular, we anticipate that their clamped-nuclei curves may allow the determination of the energy dependence of the η_{dd} defect. Here we restrict ourselves to comparing the preliminary and the new *ab initio* results with our MQDT predictions.

For the *P* state the preliminary *ab initio* potential-energy curve [7] was up to 350 cm^{-1} above the quantum-defect prediction in the region $R=1.4$ to 3.0 a.u., but in almost exact agreement with the MQDT prediction for $R=3.5$ to 5.0 a.u. (within 6 cm^{-1} over most of this region, and only 12 cm^{-1} off at $R=3.5$ a.u.). The new *ab initio* potential-energy curve [15] for the *P* state is as much as 200 cm^{-1} below the preliminary results, but despite this significant change never lies more than 2 cm^{-1} below the MQDT prediction and also maintains the agreement with the MQDT prediction in the higher R region. In fact this agreement has improved, with the calculated *ab initio* and the predicted MQDT potentials agreeing to within 2 cm^{-1} over most of the region $R=3.5$–5.0 a.u., and still only 12 cm^{-1} off at $R=3.5$ a.u. For these R values the *P* state can be identified as the $3s$ state, and it is also in this region that we have modeled the η_{ss} defect as energy independent. The fact that

the quantum-defect prediction for the P state for $R=3.5-5.0$ a.u., is in such excellent agreement with *ab initio* indicates that our modeling the η_{ss} quantum-defect function as energy independent for $R \geq 3$ a.u. is not unreasonable.

For the O state the situation is similar, although the regions are reversed. The preliminary *ab initio* results [7] agreed with the MQDT predictions to within 14 cm^{-1} in the region $R=1.4-2.3$ a.u., while lying above the MQDT results by up to 750 cm^{-1} in the region $R=2.8-5.0$ a.u. The potential-energy curve lowered by as much as 500 cm^{-1} in the new *ab initio* calculations [15], but despite this change never lies below the MQDT prediction, and in the region $R=1.4-2.3$ a.u. the agreement has actually improved, with the calculated *ab initio* and the predicted MQDT curves agreeing to within 2 cm^{-1}. The O state in the region $R=1.4-2.3$ a.u. may be identified as $4s$. The excellent agreement between the MQDT prediction and the *ab initio* calculation for the O state potential-energy curve in this region thus indicates that the simple linear energy dependence determined for the η_{ss} quantum-defect function from the lower states continues unchanged to higher energy. Combined with the equally good agreement for the large R part of the P state we see that the MQDT prediction for the newly available parts of the $3s$ and $4s$ states is extremely good. This agreement indicates that our modeling of the η_{ss} defect and its energy dependence must be close to the physical values.

In the regions for which the agreement between the MQDT prediction and the *ab initio* calculation for the P and O states is much less satisfactory these states correspond to the extremities of the $4d$ state on either side of the avoided crossings. As described above, the lack of *ab initio* data at the time we performed our fitting meant that it was not possible to determine the energy dependence of the η_{dd} defect. Despite the significance decrease in the *ab initio* calculated energies in these regions the potentials still lie as much as 220 cm^{-1} above the MQDT curves for $R=1.4-2.3$ a.u., and 370 cm^{-1} for $R=3.5-5.0$ a.u. If the *ab initio* P and O state potential-energy curves are indeed converged for all values of R, then the energy dependence of η_{dd} is not negligible and must be accounted for in the future. The difference is not necessarily due solely to an energy dependence of the η_{dd} defect, but may also involve the R dependence of the η_{dp} defect. The evidence for the convergence of the *ab initio* calculation involves experimental results for the $v=0$ level which only samples R values for $R=1.7$ to 2.5 a.u. Over this region the MQDT potential-energy function lies from 50–150 cm^{-1} below the *ab initio* potential. Yu and Dressler have used our potential curves in their calculations and Dressler has indicated to us [20] that it seems likely that our MQDT predictions for the P state curve may be about 75 cm^{-1} too low. This roughly corresponds to an average of the difference over the region sampled by $v=0$, and in fact corresponds to the difference between the two potentials at the equilibrium value of R.

Particularly significant is the fact that over large regions of R the new *ab initio* results are in closer agreement with the MQDT predictions than they are with the preliminary *ab initio* calculations. This, combined with the quality of the MQDT prediction for the $3s$ and $4s$ states, indicates the predictive power of MQDT. This is particularly shown by the fact that although the new *ab initio* results are significantly improved (and therefore changed) compared to the preliminary ones, they nevertheless remained in agreement with the MQDT in those regions where there was already agreement.

C. Diabatic and resonant states

Of particular interest in the $^1\Sigma_g^+$ state is the $(1\sigma_u)(2p\sigma_u)=(1\sigma_u)^2$ doubly excited diabatic state. At lower energies it is the interaction of this state with the singly excited states that leads to the complex series of double minima and "shouldered" potentials shown in Fig. 1. At higher energies the coupling of this doubly excited state to the singly excited $(1\sigma_g)(\epsilon s\sigma)$ and $(1\sigma_g)(\epsilon d\sigma)$ channels retains its importance, since it is responsible for electronic preionization and dissociative recombination. These continuum processes depend critically on the position of the crossing of the $(1\sigma_u)(2p\sigma_u)$ diabatic potential-energy curve with the $1s\sigma_g$ state of the ion, relative to the ionic vibrational levels. Because of this, many theoretical calculations of the $(1\sigma_u)(np\sigma_u)$ diabatic states have been performed (see Ref. [21] and citations therein). In Fig. 2, the $(1\sigma_u)(2p\sigma_u)$ diabatic potential-energy curve we obtained from the MQDT analysis of the $^1\Sigma_g^+$ bound states is compared with the *ab initio* curve of Guberman [22] (triangles connected by dashed line). The same comparison is also made for the $(1\sigma_u)(3p\sigma_u)$ state. In addition, we show the $(1\sigma_u)(2p\sigma_u)$ potential function obtained by Hazi, Derkits, and Bardsley [16] which represents a combination of *ab initio* calculation in the continuum and an MQDT parametrization of the EF and GK states. To illustrate the $(1\sigma_u)(2p\sigma_u)$ potential obtained by Hazi, Derkits, and Bardsley, we have used their *ab initio* values for energies above the ionization limit (third data row of Table I of Ref. [16]) and their MQDT parametrized values for energies below the ionization limit [Eq. (11) of Ref. [16]] Guberman's results and those of Hazi, Derkits, and Bardsley are seen to be in good agreement near the critical ionic crossing point. Other workers have obtained similar results [21]. Although they lie somewhat below these other determinations, the present MQDT results, derived from bound states lying well below the crossing, are in reasonably good agreement with them. This means that it has been possible to obtain a realistic potential-energy curve for the diabatic $(1\sigma_u)(2p\sigma_u)$ state near the ionization threshold by studying bound states lying significantly below.

The $(1\sigma_u)(3p\sigma_u)$ diabatic state is shown in Figs. 2 and 4. Both the present MQDT results and the *ab initio* results of Guberman [22] (triangles connect by a curve) are shown. The $3p$ curves predicted by these two techniques are very similar in shape, despite the fact that the $2p$ curves differ significantly for larger R values. The similarity is striking when it is remembered that our $3p$ curve is essentially an extrapolation from a fitting of the F state which lies about 30 000 cm^{-1} below. Furthermore, this

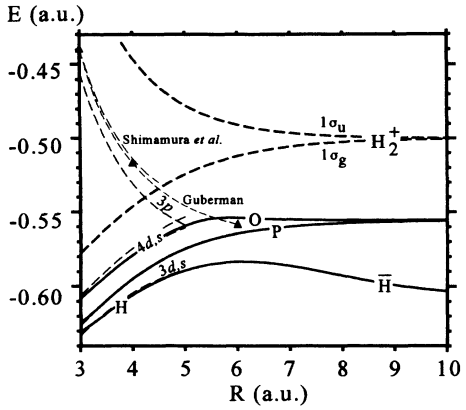

FIG. 4. Detail of the region involving the $3p$ diabatic state. *Ab initio* Born-Oppenheimer energies of the O and P states [15] (solid curves) are compared with the MQDT diabatic curves (dashed curves), and with the $3p$ diabatic curves of Guberman [22] [triangles (=data points) on faint dashed curve] and Shimamura, Noble, and Burke [21] (faint dashed curve). (Note that the $3s$ state is hidden behind the P state, and the $4d$ diabatic state is partially hidden behind the O state.) H_2^+ ion as in Fig. 1.

extrapolation had to be done without allowing for energy dependence of the η_{pp} quantum-defect function, since the lack of appropriate *ab initio* data forced us to neglect this energy dependence in the least-squares fitting. Indeed, because the $2p$ state is the first member of the p series we expect a significant energy dependence at this energy.

Another way to compare this same information is to determine η_{pp} defects using Guberman's $2p$ and $3p$ results. These are shown by the triangles and boxes, respectively, in Fig. 3(a). Comparison of the $2p$ and $3p$ versions of Guberman's η_{pp} shown in Fig. 3(a) shows that these curves are quite parallel. This implies that the energy dependence of η_{pp} is a smooth function of R, as was the case for η_{ss}. (Note that the first point of Guberman's η_{pp} quantum-defect curve for the $3p$ state is out of line with his other values.) For $R \leq 4$ a.u. the $2p$ forms of η_{pp} obtained from our MQDT analysis and from Guberman's results are gratifyingly similar. The point at $R=6$ a.u. requires some explanation. In this R region our η_{pp} curve is based on the F state. However, for large R values the F state can no longer be identified as the $2p$ state but instead corresponds to the $H^+ + H^-$ ionic state. Thus, at large R neither our η_{pp} curve nor our $2p$ diabatic curve, which are both based on the F state, correspond exactly to the diabatic p structure of Guberman's calculations. This may explain the significant difference seen at $R=6$ a.u. between the $2p$ diabatic curve determined in our MQDT calculation and that determined by Guberman (Fig. 2), and between the MQDT and Guberman versions of η_{pp} [Fig. 3(a)].

The $3p$ state will play role in avoided crossings at larger R and at higher energy than considered in this work. Figure 4 highlights the region in which these crossings should occur. The solid curves in Fig. 4 show the new *ab initio* Born-Oppenheimer potential-energy functions of Wolniewicz and Dressler [15] for the O and P states, while dashed curves show some of our diabatic curves for this same region. Because our neglect of configuration mixing starts for $R>5$ a.u., these curves only maintain their meaning out to $R \approx 5$ a.u., and are, therefore, only shown to this distance. The light dashed lines show the $3p$ state as calculated by Guberman (triangles=calculated points) and by Shimamura, Noble, and Burke [21]. According to Dressler [20], the dip in the $H\bar{H}$ state for $R \geq 6$ a.u. corresponds to the $3p$ state. Our prediction for the $3p$ state extrapolates nicely to the required position to account for this dip. The $3p$ curves of Guberman and of Shimamura do not seem to extrapolate quite so nicely, lying somewhat too high in energy.

In sweeping down to become part of the $\bar{H}$ state, the $3p$ state crosses the higher members of the s and d series. Depending on the strengths of the sp and dp interactions in this region these crossings may result in a complicated pattern of avoided crossings around $R=5$ a.u., analogous to the avoided crossing of Fig. 1 that were the object of the present work. However, this is not clearly evident in the current *ab initio* potential-energy curves for the P and O states. In the future, the detailed examination of this region may provide useful information about the off-diagonal quantum defects at larger R and to higher energy than was obtainable in the present work, along with information about the energy dependence of the η_{pp} quantum defect.

More recently, Shimamura, Noble, and Burke [21] have calculated the series of superexcited $(1\sigma_u)(np\sigma_u)$ states for $n=2-10$. Revising their Fig. 2 to plot their quantum defects as functions of ϵ for various values of R, instead of as functions of n, results in smooth curves for $\mu(\epsilon)$ for each value of R. In addition, these curves are remarkably parallel for different values of R. This further strengthens our conclusion, based on Guberman's results, that the quantum defect corresponding for the p channel has a very smooth energy dependence which is additionally uniform with R.

This energy dependence may have some effect on our prediction of the location of the crossing of the $(1\sigma_u)(2p\sigma_u)$ doubly excited state and the $1\sigma_g$ ground state of H_2^+. Future inclusion in a least-squares fitting of the new *ab initio* data for the O and P states [15] may allow us to approach the ionic crossing even more closely, from below. Indeed inclusion of the new *ab initio* data of Guberman [22], Shimamura, Noble, and Burke, [21], and other workers may well be possible and could form an important avenue for further refinement of our quantum-defect matrix.

D. Resonance widths

Shimamura, Noble, and Burke [21], as well as other authors cited there, have also used their *ab initio* wave functions for the superexcited (for $R \leq 2.6$ a.u.) doubly excited state $(1\sigma_u)(2p\sigma_u)$ to evaluate the electronic preionization width $\Gamma_e(R)$ corresponding to the decay into the $(1\sigma_g)(\epsilon s\sigma_g)$ and $(1\sigma_g)(\epsilon d\sigma_g)$ continua. We use our fitted quantum-defect matrix for the same purpose. To this end the appropriate open-channel boundary condi-

tions must be applied to the s and d channels, i.e., for these channels the effective principal quantum number ν_i in Eqs. (9) and (10) must be replaced by the continuum eigenphase τ_p and the quantity A is set to unity (see Refs. [8] and [9] for details of this procedure). Two eigenphases, $\pi\tau_\rho$, $\rho=1$, and 2, are thus obtained for each given energy above the $1\sigma_g$ threshold, and for each $R \leq 2.6$ a.u. Near the position of the $(1\sigma_u)(2p\sigma_u)$ resonance the eigenphase sum $\pi\tau=\pi\tau_1+\pi\tau_2$ rises by π. The position of the resonance is given by the point of steepest slope of the eigenphase sum, while the half width corresponds to the range over which a phase change of $\pi/4$ occurs.

We have performed this calculation at $R=2.0$ a.u. and at $R=2.5$ a.u. and our results may be compared with those of Shimamura, Noble, and Burke [21] for these two points as follows.

Present results:

$$\Gamma_e(R=2.5 \text{ a.u.})=0.060 \text{ a.u.} ,$$

$$\Gamma_e(R=2.0 \text{ a.u.})=0.024 \text{ a.u.} ;$$

ab initio [21]

$$\Gamma_e(R=2.5 \text{ a.u.})=0.0676 \text{ a.u.} ,$$

$$\Gamma_e(R=2.0 \text{ a.u.})=0.0509 \text{ a.u.} ;$$

with other *ab initio* results in substantial agreement with Shimamura, Noble, and Burke. From Fig. 2 it can be seen that the $(1\sigma_u)(2p\sigma_u)$ state crosses the $1\sigma_g H_2^+$ potential-energy curve near $R=2.6$ a.u. The excellent agreement between our width and the corresponding *ab initio* value at $R=2.5$ a.u. is gratifying since it shows once again that the present quantum-defects matrix can be realistically extrapolated to the energy range near threshold. On the other hand our prediction for the width at $R=2.0$ a.u. amounts to only half the *ab initio* value. However, at $R=2.0$ a.u. the lowest doubly excited state has risen to about 0.3 a.u. above threshold and it is not so surprising that the extrapolation from the bound-state levels used to determine the quantum-defect matrix yields less satisfactory results.

V. CONCLUSION

In this work, we have used the best quantum chemical potential-energy curves available for $^1\Sigma_g^+$ H_2 to extract a 3×3 quantum-defect matrix $\eta_{ij}(R)$ describing the e^--H_2^+ interaction including the $1\sigma_g$ and $1\sigma_u$ target states of H_2^+. We have presented arguments indicating that this matrix, beyond being a mere quantum-defect parametrization of the potential-energy curves, has enough physical content to make it useful in a wider context than that within which it was derived. Indeed, in the following paper, we shall use the η matrix determined here to calculate vibronic energies of the $^1\Sigma_g^+$ system of H_2. The results we obtain there will be within several wave-number units of experiment, despite the fact that for these levels the adiabatic and nonadiabatic non-Born-Oppenheimer effects are of the order of hundreds of wave-number units. This will be additional and strong evidence for the physicality of the η matrix.

Our approach may nevertheless appear as an unnecessary detour since it would clearly be more desirable to calculate the quantum-defect matrix *ab initio,* thus eliminating our somewhat laborious and certainly indirect fitting procedure. Yoo and Greene [23,24] have recently pursued an alternative option, evaluating the $^1\Sigma_g^+$ and $^3\Sigma_g^+$ quantum defects of H_2 in an eigenchannel R-matrix calculation formulated in prolate spherical electron coordinates. Their quantum-defect matrices reproduce the excited $^1\Sigma_g^+$ potential curves reasonably, with the inner minimum of the EF state about 100 cm^{-1} higher than in the *ab initio* calculation of Ref. [5], and the outer about 500 cm^{-1} higher. Thus, while their results cannot compete in accuracy with those of Ref. [5], they are at the very least qualitatively correct. A disturbing result of their calculations, however, is the strong and seemingly erratic energy and R dependence of the quantum defects. Indeed the energy dependence they observe is so strong as to render impossible any detailed comparison with our results. In fact it is not clear how their calculated quantum defects could be used in an MQDT calculation of vibronic energy levels, since a prerequisite for such a treatment is a smooth behavior of the quantum defects with respect to both ϵ and R. All of this is puzzling given the extreme smoothness with R of the energy dependence of the η_{ss} defect, discussed above in Sec. III C. Not only was the energy dependence of η_{ss} a smooth function of R but it also appeared to be a simple linear function of ϵ over a wide range of energy, including the $2s$, $3s$, and seemingly also the $4s$ diabatic curves, a range of about 18 000 cm^{-1}. Preliminary examination of the η_{pp} defect seems to indicate a similar smoothness with R of a simple energy dependence. It is difficult to reconcile these observations with Yoo and Greene's results. Thus, the exact relationship between their results and ours remains to be elucidated.

One important advantage of our indirect determination of the quantum-defect matrix is that from the outset we have a representation of the electronic wave function that reproduces the Born-Oppenheimer curves with a precision of a few wave-number units. It would be very difficult to obtain *ab initio* quantum-defect functions precise enough to do this, except for very highly excited states.

From this point our work will progress in several directions. First, in the following paper, we present the results of an MQDT calculation of the vibronic energies of H_2, based on the quantum-defect function determined here. Calculations of states also involving rotational excitation, and, thus, the consideration of the $3d$ complex, are already well underway, and will be presented in the third paper in this series. Finally, we plan to extend our calculations to higher energy where an increasing amount of experimental data exists on highly excited states of H_2 and on the various continuum processes involving the $(1\sigma_u)(2p\sigma_u)$ doubly excited state.

ACKNOWLEDGMENTS

S.C.R. thanks the Natural Sciences and Engineering Research Council of Canada for its continuing support of

this work through operating grants. In addition, he thanks the Laboratoire Aimé Cotton du CNRS, Orsay, France, for its hospitality and assistance during many working visits, and the Université de Paris–Sud for financial support. Dr. Kurt Dressler is especially thanked for his support, comments, and the provision of much valuable information in advance of publication, and Dr. Annick Suzor-Weiner is thanked for many useful discussions. Both of these individuals are thanked for their critical reading of the manuscript.

[1] E. R. Davidson, J. Chem. Phys. **35**, 1189 (1961).
[2] W. E. Moerner, *Persistent Spectral Hole-Burning, Science and Applications* (Springer, New York, 1988).
[3] I. F. Schneider, O. Dulieu, and A. Giusti-Suzor, J. Phys. B **24**, L289 (1991).
[4] S. Ross and Ch. Jungen, Phys. Rev. Lett. **59**, 1297 (1987).
[5] L. Wolniewicz and K. Dressler, J. Chem. Phys. **82**, 3252 (1985).
[6] P. Quadrelli, K. Dressler, and L. Wolniewicz, J. Chem. Phys. **92**, 7461 (1990).
[7] K. Dressler (private communication).
[8] Ch. Jungen and O. Atabek, J. Chem. Phys. **66**, 5584 (1977).
[9] M. J. Seaton, Rep. Prog. Phys. **46**, 167 (1983).
[10] C. H. Greene and Ch. Jungen, Adv. At. Mol. Phys. **21**, 51 (1985).
[11] S. C. Ross, in *Half Collision Resonance Phenomena in Molecules,* edited by M. García-Sucre, G. Raşeev, and S. C. Ross, AIP Conf. Proc. No. 225 (AIP, New York, 1991), pp. 73–110.
[12] H. Wind, J. Chem. Phys. **42**, 2371 (1965).
[13] D. R. Bates, K. Ledsham, and A. L. Stewart, Philos. Trans. R. Soc. London Ser. A **246**, 215 (1953).
[14] R. S. Mulliken, J. Am. Chem. Soc. **88**, 1849 (1966).
[15] L. Wolniewicz and K. Dressler, J. Chem. Phys. **100**, 444 (1994).
[16] A. U. Hazi, C. Derkits, and J. N. Bardsley, Phys. Rev. A **27**, 1751 (1983).
[17] S. Yu, K. Dressler, and L. Wolniewicz (unpublished).
[18] W. Kołos and L. Wolniewicz, J. Chem. Phys. **48**, 3672 (1968).
[19] W. Kołos and J. Rychlewski, J. Mol. Spectrosc. **143**, 212 (1990).
[20] K. Dressler (private communication).
[21] I. Shimamura, C. J. Noble, and P. G. Burke, Phys. Rev. A **41**, 3545 (1990).
[22] S. L. Guberman, J. Chem. Phys. **78**, 1404 (1983).
[23] B. Yoo, Ph.D. thesis, Louisiana State University, Baton Rouge, 1990.
[24] B. Yoo and C. H. Greene (unpublished).
[25] S. C. Ross and Ch. Jungen, following paper, Phys. Rev. A **49**, 4364 (1994).